Available online at www.sciencedirect.com
ScienceDirect
Journal of Sound and Vibration 323 (2009) 385–396
JOURNAL OF SOUND AND VIBRATION
www.elsevier.com/locate/jsvi

Analysis of frequency shifts due to thermoelastic coupling in flexural-mode micromechanical and nanomechanical resonators

Sairam Prabhakar, Michael P. Païdoussis, Srikar Vengallatore*

Department of Mechanical Engineering, McGill University, 817 Sherbrooke Street West, Montreal, QC, Canada H3A 2K6

Received 1 April 2008; received in revised form 13 November 2008; accepted 4 December 2008
Handling Editor: S. Bolton
Available online 22 January 2009

Abstract

Understanding the effects of thermoelastic coupling on the natural frequency of micro- and nanoscale resonators is essential for the design of frequency-sensitive microelectromechanical systems (MEMS). This paper presents an exact two-dimensional analysis of frequency shifts due to thermoelastic coupling in a beam undergoing flexural vibrations. The coupled heat conduction equation is solved for the thermoelastic temperature field by considering two-dimensional (2-D) heat conduction along the length and thickness of the beam. Thermoelastic coupling is modeled into the equation of motion for flexural vibrations through a temperature-dependent first moment of temperature distribution. The Galerkin technique is used to calculate the thermoelastically shifted frequencies. Detailed calculations are reported for the thermoelastic frequency shift in representative single crystal silicon and aluminum resonators over a full range of parameters. The effects of beam aspect ratio, structural boundary conditions, and mode number on the frequency shifts are discussed.

1. Introduction

Flexural-mode micromechanical and nanomechanical beam resonators are critical components of microelectromechanical systems (MEMS) used in sensing, communications, and energy harvesting. During vibration, different regions of the resonator are forced periodically into tension and compression. Due to thermoelastic coupling, these oscillating stress fields generate a time-dependent temperature field within the resonator. The coupling of elastic and thermal energy domains has two consequences: an attenuation of the amplitude of vibration due to energy dissipation, and a shift of the isothermal natural frequency. A detailed analysis of both aspects is required for the design of high performance micro- and nanoresonators.

Energy dissipation due to thermoelastic coupling manifests itself as thermoelastic damping (TED), which is defined as

$$Q_{\mathrm{TED}}^{-1} = \frac{1}{2\pi}\frac{\Delta W}{W_{\max}}, \tag{1}$$

*Corresponding author. Tel.: +1 514 398 2174.
E-mail address: srikar.vengallatore@mcgill.ca (S. Vengallatore).

0022-460X/$ - see front matter © 2008 Elsevier Ltd. All rights reserved.
doi:10.1016/j.jsv.2008.12.010

where Q_{TED}^{-1} is a dimensionless measure of TED, ΔW is the energy dissipated due to heat conduction across thermoelastic temperature gradients per cycle of vibration, and $W_{\max}$ is the maximum stored elastic energy in the vibrating structure. The effects of thermoelastic coupling on structural dynamics have been studied for over 80 years, starting with the pioneering work of Nadai in 1925 [1]. In 1937, Zener established the first theory for TED in the form of an approximate one-dimensional (1-D) analysis [2]. For a beam of thickness h vibrating at the natural frequency ω_n in the nth flexural mode, this model predicts that [2]

$$Q_{\mathrm{TED}}^{-1} = \frac{E\alpha^2 T_0}{C}\frac{\omega_n\tau}{1+(\omega_n\tau)^2} = \psi_Z\frac{\omega_n\tau}{1+(\omega_n\tau)^2}, \quad \tau = \frac{h^2 C}{\pi^2 k}; \tag{2}$$

here ψ_Z is the Zener modulus, E is theYoung's modulus, α is the linear coefficient of thermal expansion, T_0 is the equilibrium temperature of the beam, C is the specific heat per unit volume, and k is the thermal conductivity. Over the past two decades, Zener's analysis has been improved and extended in multiple directions ranging from scaling analyses [3] and single degree-of-freedom models [4] to exact theories to compute the magnitude of TED in beams [5–7], plates [8,9], rings [10], layered composite structures [11–13] and electrostatically actuated microresonators [14]. For structures with more complex geometries, numerical techniques based on the method of finite elements (FE) have been developed to compute TED [15–17].

In stark contrast, the effects of thermoelastic coupling on frequency shifts have received much less attention. The fractional shift in the natural frequency of a flexural resonator due to thermoelastic coupling is defined as [5]

$$\Delta_\omega = \frac{\omega_n - \omega_n|_{\mathrm{isothermal}}}{\omega_n|_{\mathrm{isothermal}}}; \tag{3}$$

here $\omega_n|_{\mathrm{isothermal}}$ is the isothermal value (i.e., in the absence of any thermoelastic coupling) of the natural frequency of the nth flexural mode. In 2000, Lifshitz and Roukes [5] derived a closed-form expression for the fractional frequency shift using an exact 1-D theory such that

$$\Delta_\omega = \frac{\psi_Z}{2}\left(1 - \frac{6}{\xi_n^3}\frac{\sinh\,\xi_n - \sin\,\xi_n}{\cosh\,\xi_n + \cos\,\xi_n}\right), \quad \xi_n = h\sqrt{\frac{\omega_n C}{2k}}. \tag{4}$$

Eq. (4) predicts that $\Delta_{\omega,\max} = 0.5\psi_Z$, which implies a maximal fractional frequency shift of 10^{-4} for single-crystal silicon resonators at room temperature (300 K). The analysis of Lifshitz and Roukes [5] considers heat conduction across the thickness of a vibrating Euler–Bernoulli beam. Hence, Eq. (4) does not account for the effects of length-to-thickness aspect ratio, structural boundary conditions, and mode of vibration on the frequency shift, because the analysis ignores any heat conduction along the axis of the beam. More recently, two groups—Guo and Rogerson [18], and Sun et al. [19]—presented two-dimensional (2-D) analyses of frequency shifts that considered heat conduction along the beam thickness and beam span. Both these models are approximate in the sense that they assume cubic [18] and sinusoidal [19] temperature gradients across the thickness of the beam prior to the solution of the thermoelastically-coupled equation of motion for flexural vibrations. For certain aspect ratios and boundary conditions, the 2-D models predict values as high as 10^{-3} for the fractional frequency shift in single-crystal silicon beams, thereby exceeding the predictions of the exact 1-D model by an order of magnitude. In 2007, Lepage and Golinval [20] presented a 2-D FE model for thermoelastic coupling and calculated the frequency shifts in a small set of doubly-clamped single-crystal silicon microresonators. Intriguingly, the results of the 2-D FE model were in good agreement with the exact 1-D results of Lifshitz and Roukes [5], which implies that the 2-D numerical results differ significantly from the predictions of the approximate 2-D theories.

The goal of this paper is to resolve these differences by developing an *exact* 2-D theory of frequency shifts due to thermoelastic coupling in micro- and nanomechanical resonators. The derivation of the thermoelastic equation of motion, and a framework for obtaining the solution of the thermoelastic boundary-value problem using the Galerkin method, are presented in Sections 2 and 3, respectively. In Section 4, this framework is used to compute the frequency dependence of Δ_ω for representative single-crystal silicon and aluminum resonators over a full range of parameters that include beam aspect ratios, structural boundary conditions, and mode numbers. The implications of these results for the accuracy of various 1-D and 2-D theories are discussed in Section 5.

2. Equation of motion for vibrations of a thermoelastic beam

Consider a slender, isotropic and homogeneous beam of length L, thickness h, and width b. A Cartesian coordinate system is attached to the beam such that the x-coordinate is parallel to the beam axis. The thickness and width directions are parallel to the y- and z-axes, respectively, and the structure occupies the domain defined by: $0 \leqslant x \leqslant L$; $0 \leqslant y \leqslant h$; $0 \leqslant z \leqslant b$. The beam undergoes bending vibrations of small amplitude about the x-axis, such that the deformation is consistent with the linear Euler–Bernoulli theory. The transverse displacement for vibration in the nth flexural mode with natural frequency ω_n is

$$Y(x,t) = Y_0(x)\exp(\mathrm{i}\omega_n t). \tag{5}$$

In the absence of thermoelastic coupling, the isothermal uncoupled resonance frequency is given by

$$\omega_n|_{\text{isothermal}} = \sqrt{\frac{EI}{\rho A}}\kappa_n^2, \tag{6}$$

where the constant κ_n is a function of the structural boundary conditions [21]. The goal of this analysis is to calculate the frequency shift from $\omega_n|_{\text{isothermal}}$ to ω_n due to thermoelastic coupling.

The elastic stress field in the beam is assumed to be uniaxial; only σ_{xx} can attain non-zero values. This assumption is valid for slender Euler–Bernoulli beams and neglects any shear stresses in the vicinity of clamped boundaries [22]. The time-harmonic uniaxial stress generates an oscillating temperature field due to thermoelastic coupling. The temperature field may be represented as the difference between the temperature of the beam, T, and the equilibrium temperature, T_0, as

$$\theta(x,y,t) = T(x,y,t) - T_0 = \theta_0(x,y)\exp(\mathrm{i}\omega_n t). \tag{7}$$

The amplitude θ_0 is, in general, a complex-valued quantity indicating that the temperature field is not in phase with the applied stress.

The equation of motion for this vibrating beam is obtained by combining geometric relationships with thermoelastic constitutive laws. From the generalized Hooke's law of linear thermoelasticity, the strain field in the beam is [23]

$$\varepsilon_{xx} = \frac{\sigma_{xx}}{E} + \alpha\theta, \quad \varepsilon_{yy} = \varepsilon_{zz} = \alpha\theta. \tag{8}$$

All other strain components are identically zero.

The relation between strain and displacement is based purely on geometrical arguments and is the same for both thermoelasticity and isothermal elasticity [23]. Therefore, the strain-curvature relationship for an Euler–Bernoulli beam in flexure is

$$\varepsilon_{xx} = -(y - h/2)\frac{\partial^2 Y}{\partial x^2}. \tag{9}$$

Eqs. (8) and (9) can be combined to yield

$$\sigma_{xx} = -E(y - h/2)\frac{\partial^2 Y}{\partial x^2} - E\alpha\theta. \tag{10}$$

From Newton's second law, the equation of motion for free flexural vibrations of the beam is

$$\frac{\partial^2 M_z}{\partial x^2} + \rho A\frac{\partial^2 Y}{\partial t^2} = 0, \tag{11}$$

where A is the cross-sectional area of the beam and ρ its density. The internal moment, M_z, is given by

$$M_z = -\int_0^b \int_0^h (y - h/2)\sigma_{xx}\,\mathrm{d}y\,\mathrm{d}z = EI\frac{\partial^2 Y}{\partial x^2} + EI_T\alpha, \tag{12}$$

where the mechanical moment of inertia, I, and the first moment of temperature distribution, I_T, are defined as

$$I = \frac{bh^3}{12}, \tag{13a}$$

$$I_T = b\int_0^h (y - h/2)\theta \, dy. \tag{13b}$$

Finally, the coupled equation of motion is obtained by substituting Eq. (12) in Eq. (11) to give

$$EI\frac{\partial^4 Y}{\partial x^4} + E\alpha\frac{\partial^2 I_T}{\partial x^2} + \rho A\frac{\partial^2 Y}{\partial t^2} = 0. \tag{14}$$

At this stage, we proceed by first solving a thermal boundary-value problem to obtain expressions for the time-harmonic temperature field, θ, and the first moment of temperature distribution, I_T. With this, the equation of motion, Eq. (14), can be solved subject to the appropriate structural boundary conditions to determine the natural frequency, ω_n, for thermoelastically-coupled vibrations in the nth mode. The next section describes the detailed implementation of this approach within the context of a 2-D theory of classical thermoelasticity.

3. 2-D analysis of thermoelastic coupling

3.1. Analysis of the thermal field

The analysis presented in this section closely follows the framework developed recently to establish a 2-D theory of TED [7]. The starting point is the coupled equation for heat conduction within the vibrating beam [23,24]

$$C\frac{\partial\theta}{\partial t} = k\nabla^2\theta - E\alpha T_0\frac{\partial\varepsilon_{xx}}{\partial t}. \tag{15}$$

Eq. (15) ignores the contributions from the transverse strains ε_{yy} and ε_{zz}. We have demonstrated that the errors caused by this omission are negligible [7].

The 2-D analysis considers heat conduction due to temperature gradients along the span (x-) and across the thickness (y-) of the beam. Hence, Eq. (15) reduces to

$$C\frac{\partial\theta}{\partial t} = k\left(\frac{\partial^2\theta}{\partial x^2} + \frac{\partial^2\theta}{\partial y^2}\right) - E\alpha T_0\frac{\partial\varepsilon_{xx}}{\partial t}. \tag{16}$$

Eq. (16) can be solved using the method of Green's functions subject to the appropriate thermal boundary conditions [25]. These thermal conditions must be defined at the extremities of the beam axis ($x = 0,L$), and at the lateral bounding surfaces of the beam ($y = 0,h$). For the structures considered in this paper, these surfaces are either free (surrounded by a gas at low pressure) or clamped to a substrate. The substrate is much larger than the beam, and the clamped surface is modeled as being in perfect thermal contact with the substrate. Therefore, a clamped end of the beam corresponds to an isothermal boundary condition. For free surfaces, radiation is the only mechanism of heat transfer, and the rate of radiative heat transfer scales as the difference between the fourth powers of the absolute temperatures of the beam and the surroundings [25]. For micro- and nanomechanical resonators operating at room temperature (300 K), the maximum change in temperature due to thermoelastic coupling is $\sim$0.1 K [7]. Therefore, radiation from free surfaces is negligible, and these surfaces correspond to an adiabatic thermal boundary condition [5–14].

Thus, the thickness coordinate thermal boundary conditions for the doubly-clamped beam as well as the cantilever are adiabatic,

$$\left.\frac{\partial\theta}{\partial y}\right|_{y=0,h} = 0. \tag{17}$$

The span coordinate thermal boundary conditions for a doubly-clamped beam are isothermal,

$$\theta|_{x=0,L} = 0. \tag{18}$$

For the cantilever, the fixed end ($x = 0$) is in perfect thermal contact with the substrate and hence isothermal. Therefore,

$$\theta|_{x=0} = 0. \tag{19a}$$

The free end ($x = L$) of the cantilever is adiabatic, and therefore

$$\left.\frac{\partial\theta}{\partial x}\right|_{x=L} = 0. \tag{19b}$$

Based on these boundary conditions, the temperature change due to thermoelastic coupling is calculated as the complex-valued quantity

$$\theta_{2D}(x, y, \omega_n, t) = (\theta^R_{2D}(x, y, \omega_n) + \mathrm{i}\theta^I_{2D}(x, y, \omega_n)) \exp(\mathrm{i}\omega_n t). \tag{20a}$$

The real and imaginary parts of the temperature field are given by

$$\begin{aligned}
\theta^R_{2D} &= \frac{4E\alpha T_0}{C}\frac{1}{Lh}\sum_{m=1}^{\infty}\sum_{p=1}^{\infty}\frac{\omega_n^2}{\omega_n^2+\frac{k^2}{C^2}(\beta_m^2+\gamma_p^2)^2}\chi_m\eta_p\ \sin(\beta_m x)\ \cos(\gamma_p y),\\
\theta^I_{2D} &= \frac{4E\alpha T_0}{C}\frac{1}{Lh}\sum_{m=1}^{\infty}\sum_{p=1}^{\infty}\frac{\omega_n\frac{k}{C}(\beta_m^2+\gamma_p^2)}{\omega_n^2+\frac{k^2}{C^2}(\beta_m^2+\gamma_p^2)^2}\chi_m\eta_p\ \sin(\beta_m x)\ \cos(\gamma_p y),
\end{aligned} \tag{20b}$$

where

$$\begin{aligned}
\chi_m &= \int_{x'=0}^{L}\sin(\beta_m x')\frac{\partial^2 Y}{\partial x'^2}\mathrm{d}x',\\
\eta_p &= \int_{y'=0}^{h}\cos(\gamma_p y')(y' - h/2)\,\mathrm{d}y';
\end{aligned} \tag{20c}$$

the primes within the integral denote dummy variables. The eigenvalues are

$$\gamma_p = \frac{p\pi}{h}, \quad p = 0, 1, 2, \ldots$$

$$\beta_m = \begin{cases} \dfrac{2m-1}{2}\dfrac{\pi}{L},\ m = 1, 2, \ldots & \text{for a cantilever}\\ \dfrac{m\pi}{L},\ m = 1, 2, \ldots & \text{for a doubly clamped beam}\end{cases} \tag{20d}$$

This completes the determination of the temperature field within the beam.

3.2. Solution of the coupled equation of motion

The first moment of temperature distribution, I_T, can be calculated from Eq. (13b) using the values of θ from Eq. (20). Substituting I_T into Eq. (14), the equation of motion with 2-D heat conduction is obtained as

$$EI\frac{\partial^4 Y}{\partial x^4} + \rho A\frac{\partial^2 Y}{\partial t^2} - \frac{4E\alpha T_0}{C}\frac{b}{Lh}\sum_{m=1}^{\infty}\sum_{p=1}^{\infty}(R_{mp}|_{\omega_n} + \mathrm{i}I_{mp}|_{\omega_n})\exp(\mathrm{i}\omega_n t) = 0, \tag{21a}$$

with

$$R_{mp}|_{\omega_n} = \frac{\beta_m^2\omega_n^2}{\omega_n^2 + \dfrac{k^2}{C^2}(\beta_m^2+\gamma_p^2)^2}\chi_m\eta_p^2\ \sin(\beta_m x),$$

$$I_{mp}|_{\omega_n} = \frac{\beta_m^2 \omega_n \dfrac{k}{C}(\beta_m^2 + \gamma_p^2)}{\omega_n^2 + \dfrac{k^2}{C^2}(\beta_m^2 + \gamma_p^2)^2} \chi_m \eta_p^2 \sin(\beta_m x); \tag{21b}$$

here R_{mp} and I_{mp} represent the thermoelastic coupling terms for the beam undergoing flexural vibrations in the nth mode. The real and imaginary parts are measures of the frequency shift and energy dissipation, respectively [5]. The notation $(|_{\omega_n})$ makes explicit that both terms are evaluated at the thermoelastically shifted natural frequency ω_n for the specific mode under consideration.

Eq. (21a) is implicit in ω_n because the coupling terms R_{mp} and I_{mp} are themselves functions of the natural frequency. Therefore, an iterative solution procedure based on the weighted residual Galerkin technique [26] is used to calculate ω_n from a spatially-discretized form of the equation of motion. The first step is the selection of an approximate solution

$$Y(x,t) \approx Y_N(x,t) = \sum_{r=1}^{N} \phi_r(x) q_r(t). \tag{22}$$

The comparison functions $\phi_r(x)$ satisfying the beam boundary conditions are taken to be the eigenfunctions of the beam,

$$\phi_r(x) = \cosh(\kappa_r x) - \cos(\kappa_r x) - \vartheta_r(\sinh(\kappa_r x) - \sin(\kappa_r x)). \tag{23}$$

The constants κ_r and ϑ_r depend upon the structural boundary conditions of the beam [21]. The temporal function for harmonic flexural vibrations with modal resonance frequencies ω_r (the shifted frequency due to thermoelastic coupling) is

$$q_r(t) = \exp(\mathrm{i}\omega_r t), \quad r = 1, 2, \ldots, N. \tag{24}$$

The residual (i.e., the error induced by the approximate solution) in the equation of motion is

$$\Re = EI \frac{\partial^4 Y_N}{\partial x^4} + \rho A \frac{\partial^2 Y_N}{\partial t^2} - \frac{4E\alpha T_0}{C} \frac{b}{Lh} \sum_{m=1}^{\infty} \sum_{p=1}^{\infty} (R_{mp}|_{\omega_n} + \mathrm{i} I_{mp}|_{\omega_n}) \exp(\mathrm{i}\omega_n t). \tag{25}$$

Next, the approximate solution of Eq. (22) is constrained to satisfy the equation of motion in an average sense such that the weighted average of the residual, with a suitable weighting function, goes to zero over the domain $0 \leqslant x \leqslant L$. For the Galerkin method, the weighting function has the same form as the spatial approximation of the solution, $\phi_j(x)$, $\quad j = 1, 2, \ldots, N$. The Galerkin criterion is

$$\int_0^L \Re \phi_j \, \mathrm{d}x = 0, \quad j = 1, 2, \ldots, N. \tag{26}$$

Evaluating this integral using the definition of q_r from Eq. (24), and invoking the orthogonality of the beam eigenfunctions $\phi(x)$, the N spatially discretized equations of motion are obtained as

$$\sum_{r=1}^{N} (EI\kappa_r^4 L \delta_{rj} - \rho A L \delta_{rj} \omega_r^2) \exp(\mathrm{i}\omega_r t) - \frac{4E\alpha T_0}{C} \frac{b}{Lh} \sum_{m=1}^{\infty} \sum_{p=1}^{\infty} \int_0^L (R_{mp}|_{\omega_n} + \mathrm{i} I_{mp}|_{\omega_n}) \phi_j \, \mathrm{d}x \exp(\mathrm{i}\omega_n t) = 0, \quad j = 1, \ldots, N \tag{27}$$

where δ_{rj} is the Kronecker delta.

The thermoelastic coupling term is independent of the transverse amplitude of vibrations, Y, and this system of equations yields a single equation for ω_n, namely

$$\omega_n^2 = \frac{EI}{\rho A} \kappa_n^4 - \frac{4E\alpha T_0}{C\rho} \frac{1}{L^2 h^2} \sum_{m=1}^{\infty} \sum_{p=1}^{\infty} \int_0^L (R_{mp}|_{\omega_n} + \mathrm{i} I_{mp}|_{\omega_n}) \phi_n \, \mathrm{d}x. \tag{28}$$

Using the definition of $\omega_n|_{\text{isothermal}}$ from Eq. (6) in Eq. (28) yields

$$\omega_n^2 = \omega_n|_{\text{isothermal}}^2 - \frac{4E\alpha T_0}{C\rho}\frac{1}{L^2h^2}\sum_{m=1}^{\infty}\sum_{p=1}^{\infty}\int_0^L (R_{mp}|_{\omega_n} + \mathrm{i}I_{mp}|_{\omega_n})\phi_n \,\mathrm{d}x. \tag{29}$$

Eq. (29) is a nonlinear algebraic equation in ω_n, and can be solved using an iterative technique.

As a first approximation, $R_{mp}|_{\omega_n}$and $I_{mp}|_{\omega_n}$ are calculated from Eq. (21b) by setting $\omega_n = \omega_n|_{\text{isothermal}}$. Next, Eq. (29) is solved for ω_n, following which $R_{mp}|_{\omega_n}$and $I_{mp}|_{\omega_n}$ are re-calculated using the new value of ω_n. While evaluating Eq. (29), we found that the infinite summation associated with $R_{mp}|_{\omega_n}$ and $I_{mp}|_{\omega_n}$ converges within 200 terms ($m = p = 200$) for all the cases studied in this paper. Subsequently a refined value of the natural frequency is obtained by solving Eq. (29). This process is continued until the value of ω_n used to calculate $R_{mp}|_{\omega_n}$ and $I_{mp}|_{\omega_n}$ in Eq. (21b) is within a specified numerical tolerance of the value that emerges from the solution of Eq. (29). For the kth iteration (with $k = 0$ corresponding to the initial approximation where $\omega_n = \omega_n|_{\text{isothermal}}$), the fractional error, $\varepsilon^{(k)}$, in the iterative calculation of the complex valued frequency, $\omega_n{}^{(k)}$, at that step of iteration is defined as

$$\varepsilon^{(k)} = \frac{\mathrm{Re}(\omega_n^{(k)}) - \mathrm{Re}(\omega_n^{(k-1)})}{\mathrm{Re}(\omega_n^{(k-1)})}. \tag{30}$$

If k^* is the iteration step at which the error $\varepsilon^{(k^*)}$drops below the selected stopping tolerance, then the iterative process is terminated, and the dimensionless fractional frequency shift due to thermoelastic coupling is calculated as

$$\Delta_\omega = \frac{\mathrm{Re}(\omega_n^{(k^*)}) - \omega_n|_{\text{isothermal}}}{\omega_n|_{\text{isothermal}}}. \tag{31}$$

This completes the algorithm for computing the frequency dependence of the frequency shift. Results from the implementation of this numerical procedure are presented next to compute the frequency dependence of Δ_ω.

4. Numerical results for frequency shifts

The theoretical framework presented in the previous section is used here to compute the frequency dependence of Δ_ω over a full range of parameters. The results are organized as follows. First, we consider the case of single-crystal silicon and compute the effects of beam aspect ratio and structural boundary conditions on the frequency shift. The properties of the iterative solution are discussed and detailed comparisons are made with the 2-D FE results of Lepage and Golinval [20] to validate the theory. Next, the accuracy of the exact 1-D theory is assessed by comparison with the exact 2-D results for the frequency dependence of Δ_ω for different structural boundary conditions (cantilevered and doubly-clamped beams), beam aspect ratios, and material properties (single-crystal silicon and aluminum). The following values were used for the material properties of single-crystal silicon: $E = 160\,\text{GPa}$, $\alpha = 2.6\times10^{-6}\,\text{K}^{-1}$, $C = 1.6\times10^{6}\,\text{J m}^{-3}\,\text{K}^{-1}$, $k = 150\,\text{W m}^{-1}\,\text{K}^{-1}$, $\rho = 2300\,\text{kg m}^{-3}$, and $\psi_Z = 2\times10^{-4}$ at 300 K [12]. The corresponding values for aluminum are: $E = 70\,\text{GPa}$, $\alpha = 24\times10^{-6}\,\text{K}^{-1}$, $C = 2.4\times10^{6}\,\text{J m}^{-3}\,\text{K}^{-1}$, $k = 220\,\text{W m}^{-1}\,\text{K}^{-1}$, $\rho = 2700\,\text{kg m}^{-3}$, and $\psi_Z = 5\times10^{-3}$ at 300 K [12].

4.1. Convergence and comparison with 2-D FEM

Fig. 1 shows the results of iterative calculation of Eq. (29) for silicon cantilevers vibrating in the first flexural mode. The thickness of the beams ranges from 100 nm to 100 μm, and the length-to-thickness aspect ratio is fixed at $L/h = 10$ for all beams. The fractional error ε defined in Eq. (30) attains values less than 10^{-13} within two iterations. Subsequently, the fractional frequency shift due to thermoelastic coupling can be calculated using Eq. (31).

Fig. 2 compares the computed values of frequency shift for the fundamental-mode vibrations of doubly-clamped single-crystal silicon beams with thickness ranging from 3 to 9 μm, and a fixed length of $L = 90\,\mu\text{m}$. Also shown for comparison are the corresponding results extracted from a 2-D FE study by Lepage and Golinval [20]. The numerical procedure was implemented using quadrilateral plane stress elements with a 2-D

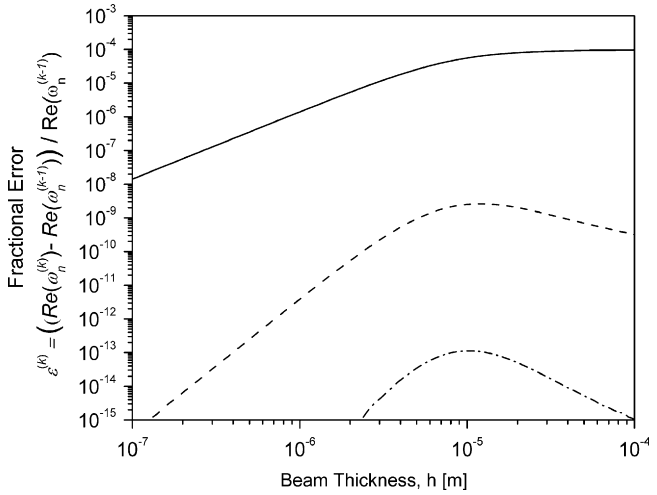

Fig. 1. Variation of fractional error $\varepsilon^{(k)}$ associated with the iterative solution of Eq. (29) for the frequency shift. These results are for the representative case of a single-crystal silicon cantilever of aspect ratio $L/h = 10$ vibrating in the first flexural mode: ———, initial approximation ($k = 0$); - - - - - - -, first iteration ($k = 1$); and - · - · - · - · -, second iteration ($k = 2$).

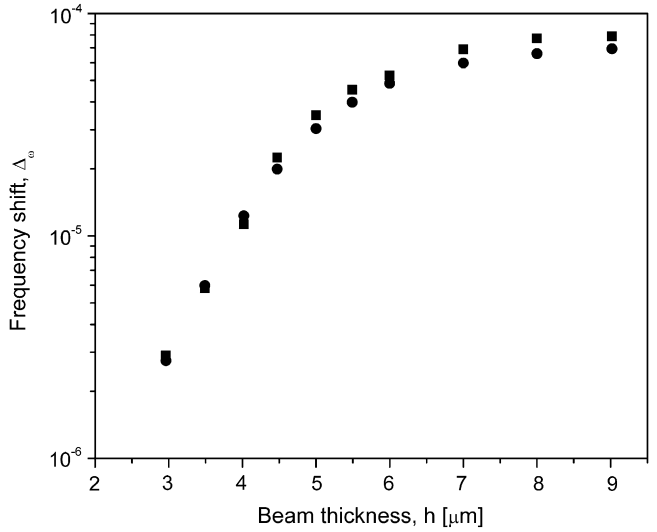

Fig. 2. Comparison of frequency shifts computed using our exact 2-D theory with the results of the 2-D finite-element analysis presented by Lepage and Golinval [20]. All results are for doubly-clamped single-crystal silicon beams of length $L = 90\,\mu m$ vibrating in the first flexural mode: ●, results from the exact 2-D theory; and ■, results of the 2-D finite element analysis.

temperature field along the span and across the thickness of a silicon flexural resonator in that study. In all cases, the results from the exact 2-D theory and the 2-D FE analysis differ by less than 13%.

4.2. *Effects of aspect ratio and boundary conditions*

The graphs in Figs. 3 and 4 show the fractional frequency shift as a function of the normalized frequency ξ_n for single-crystal silicon resonators computed using the exact 2-D theory. For comparison, the results of the exact 1-D theory of Lifshitz and Roukes [5] are also shown. Fig. 3 shows the effect of beam aspect ratio on the frequency shift for doubly-clamped beams vibrating in the first flexural mode. The frequency shift varies monotonically between zero (in the low frequency limit) and attains a maximum value of 10^{-4} with increasing ξ_n.

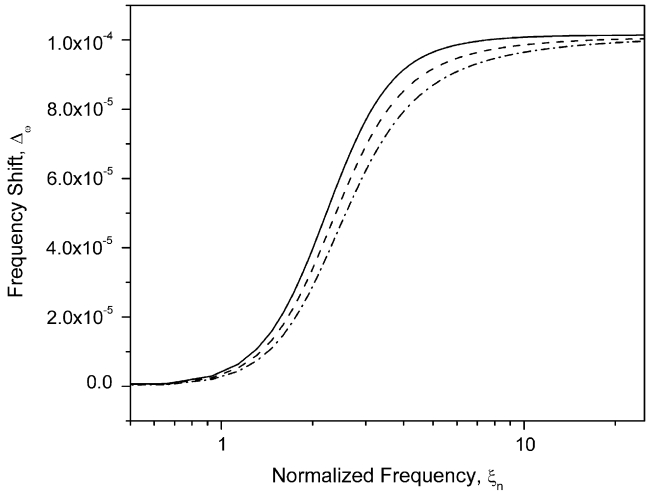

Fig. 3. Effect of beam aspect ratio on frequency shift in doubly-clamped single-crystal silicon beams vibrating in the first mode. These results are calculated using the exact 2-D theory: - - - - - - - - -, $L/h = 10$; - - - - - - -, $L/h = 20$; and ——, $L/h \geqslant 40$, converging to the exact 1-D theory of Lifshitz and Roukes [5] in the limit $L/h \to \infty$.

This maximum value corresponds to the asymptotic limit of $0.5\psi_Z$ predicted by Lifshitz and Roukes [5]. The differences between the 2-D and 1-D theories are maximum for short stubby beams with low aspect ratio of $(L/h) = 10$. However, as the aspect ratio increases, the differences between the two theories diminish, and the exact 1-D theory is accurate to within 10% for long slender beams with $(L/h) \geqslant 40$.

Fig. 4(a) shows the frequency dependence of the fractional frequency shift in single-crystal silicon beams with aspect ratio of $(L/h) = 10$ computed using the exact 2-D theory. Results are shown for cantilevered and doubly-clamped beams vibrating in the first flexural mode. The solid line in the graph corresponds to the predictions of the exact 1-D theory [5]. Fig. 4(b) shows the relative error, $(\Delta_\omega^{1D}/\Delta_\omega^{2D}) - 1$, between the exact 1-D and 2-D theories. The 1-D theory incurs a maximum error of 50% in doubly-clamped beams, which is twice the corresponding value for cantilevered beams, for frequencies of $\xi_n < 1$. However, the relative error is negligible at high frequencies ($\xi_n > 10$).

Fig. 5(a) shows the frequency dependence of the fractional frequency shift for doubly-clamped aluminum beams vibrating in the first flexural mode, with different (L/h) aspect ratios. The relative error between the exact 1-D and 2-D theories is shown in Fig. 5(b). The results correspond closely with those for single-crystal silicon: (i) the frequency shift ranges from zero to $0.5\psi_Z$; (ii) the exact 1-D theory is accurate for long slender beams with aspect ratios of $(L/h) \geqslant 40$; (iii) the maximum error in the exact 1-D theory is 50% and occurs for doubly-clamped beams of low aspect ratio of $(L/h) = 10$.

The exact 2-D theory was also used to compute the thermoelastic frequency shift for beams resonating in higher flexural modes. For cantilevers and doubly-clamped beams vibrating in the second flexural mode, the frequency shift is within 1% of that corresponding to the fundamental mode.

5. Discussion and conclusions

This paper presented an exact 2-D theory to compute the effects of thermoelastic coupling on frequency shifts by accounting for heat conduction along the span, and across the thickness, of vibrating Euler–Bernoulli beams. The theoretical framework closely follows the formulation developed by Prabhakar and Vengallatore [7] to compute thermoelastic damping in micro- and nanomechanical resonators. This framework is based on classical continuum thermomechanics and assumes that heat transfer is diffusive (and not ballistic), which requires the structural dimensions to exceed the mean free path of the quanta of heat transport [5].

The 2-D formulation leads to a coupled equation of motion, which was solved using the Galerkin method to compute the effects of thermoelastic coupling on the frequency shift. The results of the exact 2-D theory were

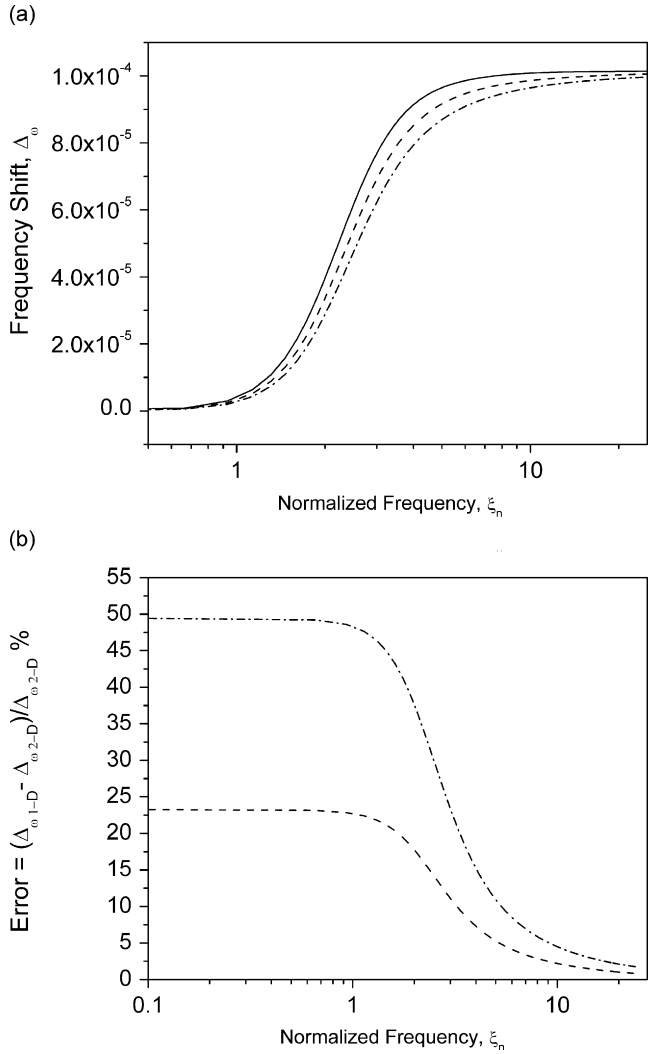

Fig. 4. Effect of structural boundary conditions on frequency shift in single-crystal silicon beams with $L/h = 10$ vibrating in the first flexural mode: (a) frequency shift computed using the exact 2-D theory for cantilevered (- - - - - - -) and doubly-clamped (- · - · - · - · -) beams. For comparison, the frequency shift predicted by the exact 1-D theory of Lifshitz and Roukes [5] is indicated by the solid line. (b) The error in the exact 1-D theory relative to the exact 2-D theory for cantilevered beams (- - - - - - -) and doubly-clamped beams (- · - · - · - · -) with $L/h = 10$ vibrating in the first flexural mode.

shown to be in good agreement with the 2-D FE analysis of Lepage and Golinval [20], which serves to validate the computational procedure used here.

A second, and complementary, aspect of validation emerges from a comparison of the limiting values of the exact 2-D theory with those predicted by the exact 1-D theory of Lifshitz and Roukes [5]. The 1-D theory considers heat conduction only across the beam thickness and does not impose thermal boundary conditions at the ends of the beam span. The errors due to both factors are expected to diminish in importance as the slenderness of the beam increases [7], such that the 1-D and 2-D theories are expected to converge in the limit of large aspect ratio. In addition, for a given aspect ratio, the differences between the two theories for doubly-clamped beams with two isothermal axial boundaries are expected to be greater than those for cantilevers. The results shown in Figs. 3 and 4 are consistent with these expectations.

The exact 1-D theory is convenient since it leads to a simple closed-form expression for the fractional frequency shift. This expression is accurate for long slender beams but can lead to significant errors for

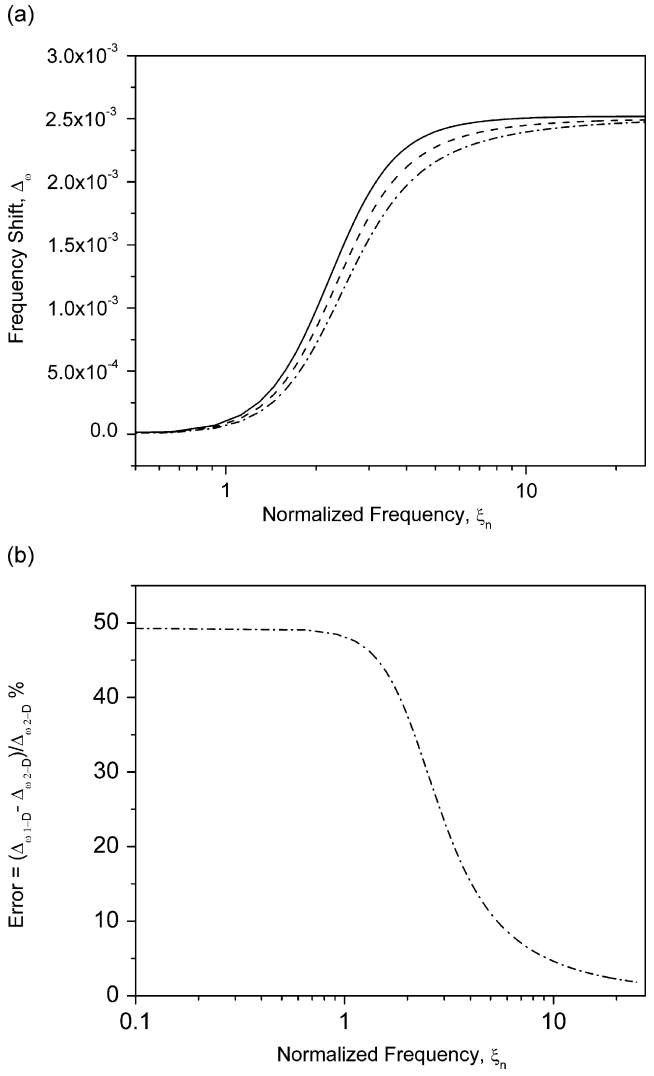

Fig. 5. Frequency shifts in doubly-clamped aluminum beams computed using the exact 2-D theory: (a) vibrations in the first flexural mode, - · - · - · -, $L/h = 10$; - - - - - - -, $L/h = 20$; and ——, $L/h \geqslant 40$, converging to the exact 1-D theory of Lifshitz and Roukes [5] in the limit $L/h \to \infty$. (b) The error in the exact 1-D theory relative to the exact 2-D theory for doubly-clamped aluminum beams with $L/h = 10$ vibrating in the first flexural mode.

beams with low aspect ratio. The maximum error of 50% occurs for doubly-clamped beams with $(L/h) = 10$. In such cases, the use of the exact 2-D theory is necessary for an accurate computation of the frequency shift. Our results, as well as those of Lifshitz and Roukes [5] and Lepage and Golinval [20], are consistent with a maximal value of $0.5\psi_Z$ for Δ_ω. This result implies that the approximate 2-D models of Guo and Rogerson [18] and Sun et al. [19] can overestimate the fractional frequency shift by an order of magnitude.

An examination of the sign of Δ_ω is instructive because of its implications for the stability of vibrations. In all cases, Figs. 3–5 show that thermoelastic coupling leads to an increase of the natural frequency. Thus, thermoelastic coupling effectively leads to an increase in the stiffness of the structure. This stabilizing effect is in contrast to other types of coupling (such as fluid-elastic coupling [26]) which lead to a softening of the beam and hence to static or dynamic instabilities.

Acknowledgments

The authors gratefully acknowledge financial support from the Natural Sciences and Engineering Research Council (NSERC) of Canada, General Motors of Canada, Inc., and the Canada Research Chairs program.

References

[1] A. Nadai, *Die Elastische Platten*, Julius Springer, Berlin, 1925.
[2] C. Zener, Internal friction in solids, I. Theory of internal friction in reeds, *Physical Review* 52 (1937) 230–235.
[3] V.T. Srikar, S.D. Senturia, Thermoelastic damping in fine-grained polysilicon flexural beam resonators, *Journal of Microelectromechanical Systems* 11 (2002) 499–504.
[4] J. Rajagopalan, M.T.A. Saif, Single degree of freedom model for thermoelastic damping, *Journal of Applied Mechanics* 74 (2007) 461–468.
[5] R. Lifshitz, M.L. Roukes, Thermoelastic damping in micro- and nanomechanical systems, *Physical Review B* 61 (2000) 5600–5609.
[6] V.K. Kinra, K.B. Milligan, A second-law analysis of thermoelastic damping, *Journal of Applied Mechanics* 61 (1994) 71–76.
[7] S. Prabhakar, S. Vengallatore, Theory of thermoelastic damping in micromechanical resonators with two-dimensional heat conduction, *Journal of Microelectromechanical Systems* 17 (2008) 494–502.
[8] A.H. Nayfeh, M.I. Younis, Modeling and simulations of thermoelastic damping in microplates, *Journal of Micromechanics and Microengineering* 14 (2004) 1711–1717.
[9] A.N. Norris, Dynamics of thermoelastic thin plates: a comparison of four theories, *Journal of Thermal Stresses* 29 (2006) 169–195.
[10] S.J. Wong, C.H.J. Fox, S. McWilliam, Thermoelastic damping of the in-plane vibration of thin silicon rings, *Journal of Sound and Vibration* 293 (2006) 266–285.
[11] J.E. Bishop, V.K. Kinra, Elastothermodynamic damping in laminated composites, *International Journal of Solids and Structures* 34 (1997) 1075–1092.
[12] S. Vengallatore, Analysis of thermoelastic damping in laminated composite micromechanical beam resonators, *Journal of Micromechanics and Microengineering* 15 (2005) 2398–2404.
[13] S. Prabhakar, S. Vengallatore, Thermoelastic damping in bilayered micromechanical beam resonators, *Journal of Micromechanics and Microengineering* 17 (2007) 532–538.
[14] S.K. De, N.R. Aluru, Theory of thermoelastic damping in electrostatically actuated microstructures, *Physical Review B* 74 (2006) 144305.
[15] A. Duwel, R.N. Candler, T.W. Kenny, M. Varghese, Engineering MEMS resonators with low thermoelastic damping, *Journal of Microelectromechanical Systems* 15 (2006) 1437–1445.
[16] M.J. Silver, L.D. Peterson, R.S. Erwin, Predictive elastothermodynamic damping in finite element models using a perturbation formulation, *AIAA Journal* 43 (2005) 2646–2653.
[17] Y.B. Yi, M.A. Matin, Eigenvalue solution of thermoelastic damping in beam resonators using a finite element analysis, *Journal of Vibration and Acoustics* 129 (2007) 478–483.
[18] F.L. Guo, G.A. Rogerson, Thermoelastic coupling effect on a micro-machined beam resonator, *Mechanics Research Communications* 30 (2003) 513–518.
[19] Y. Sun, D. Fang, A.K. Soh, Thermoelastic damping micro-beam resonators, *International Journal of Solids and Structures* 43 (2006) 3213–3229.
[20] S. Lepage, J. Golinval, Finite element modeling of thermoelastic damping in filleted micro-beams, *Proceedings of IEEE EuroSimE 2007*, London, April 2007, pp. 1–7.
[21] M.L. James, G.M. Smith, J.C. Wolford, P.W. Whaley, *Vibration of Mechanical and Structural Systems with Microcomputer Applications*, Harper and Row, New York, 1989.
[22] V.T. Srikar, A.K. Swan, M.S. Unlu, B.B. Goldberg, S.M. Spearing, Micro-Raman measurement of bending stresses in micromachined silicon flexures, *Journal of Microelectromechanical Systems* 12 (2003) 779–787.
[23] B.A. Boley, J.H. Wiener, *Theory of Thermal Stresses*, Wiley, New York, 1960.
[24] J.L. Nowinski, *Theory of Thermoelasticity with Applications*, Sijthoff and Noordhoff, Amsterdam, 1978.
[25] M.N. Ozisik, *Heat Conduction*, Wiley, New York, 1980.
[26] M.P. Païdoussis, *Fluid-Structure Interactions: Slender Structures and Axial Flow*, Vol. 1, Academic Press, San Diego, 1998.